Long-Term Stability of Thin-Film Pd-Based Supported Membranes

**Niek de Nooijer [1], Alba Arratibel Plazaola [2], Jon Meléndez Rey [2], Ekain Fernandez [2],
David Alfredo Pacheco Tanaka [2], Martin van Sint Annaland [1] and Fausto Gallucci [1,*]**

[1] Department of Chemical Engineering and Chemistry, Eindhoven University of Technology, De Rondom 70, 5612 AZ Eindhoven, The Netherlands; n.c.a.d.nooijer@tue.nl (N.d.N.); m.v.sintannaland@tue.nl (M.v.S.A.)
[2] Tecnalia Energy and Environment Division. Mikeletegi Pasealekua 2, 20009 San Sebastian-Donostia, Spain; alba.arratibel@tecnalia.com (A.A.P.); jon.melendez@tecnalia.com (J.M.R.); ekain.fernandez@tecnalia.com (E.F.); alfredo.pacheco@tecnalia.com (D.A.P.T.)
*   Correspondence: f.gallucci@tue.nl

check for updates

Abstract: Membrane reactors have demonstrated a large potential for the production of hydrogen via reforming of different feedstocks in comparison with other reactor types. However, the long-term performance and stability of the applied membranes are extremely important for the possible industrial exploitation of these reactors. This study investigates the long-term stability of thin-film Pd-Ag membranes supported on porous Al_2O_3 supports. The stability of five similarly prepared membranes have been investigated for 2650 h, up to 600 °C and in fluidized bed conditions. Results show the importance and the contribution of the sealing of the membranes at temperatures up to 500 °C. At higher temperatures the membranes surface deformation results in pinhole formation and a consequent decrease in selectivity. Stable operation of the membranes in a fluidized bed is observed up to 450 °C, however, at higher temperatures the scouring action of the particles under fluidization causes significant deformation of the palladium surface resulting in a decreased selectivity.

Keywords: Palladium based membranes; membrane stability; membrane reactors; fluidized bed; hydrogen production

1. Introduction

The increasing demand for the reduction of greenhouse gas (GHG) emissions has increased interest in hydrogen as an energy carrier, as it does not have any GHG emissions at the end-user. However, steam reforming of natural gas, the conventional production method for hydrogen, produces significant GHG emissions. In order to reduce these emissions for the production of hydrogen, novel and improved reforming processes are being proposed, such as more active catalyst, new reactor design resulting in higher conversions and improved efficiencies. In addition to these process intensification alternatives, use of sustainable fuel sources is also proposed, such as bio-methanol, bio-ethanol and biogas [1].

Palladium-based membrane technology has shown great potential in improving the reforming efficiency and intensifying the reforming processes [2]. The membranes can either be applied as a downstream separation step for hydrogen or integrated with the catalyst in a membrane reactor, in which hydrogen production and separation are combined in one step. Membrane reactors are mostly studied in two different configurations, viz. (micro) packed bed (PB) and fluidized bed (FB) reactors. The membranes allow for the selective extraction of hydrogen from the reactor, shifting the equilibrium, thereby resulting in a higher conversion at lower temperatures (and consequently higher efficiency).

This produces a stream of pure hydrogen directly from the reactor without the need for down-stream separations. Long-term stable production of pure hydrogen is therefore imperative to make the concept of membrane reactors feasible. The performance of a membrane reactor depends largely on the flux of hydrogen extracted and on the purity of the hydrogen produced. The stability of a membrane is here considered as the ability of a membrane to maintain a constant flux of hydrogen, as well as a constant perm-selectivity over time.

The performance of different membranes and membrane reactor configurations has been reported in the literature. Full conversions of the feedstock, as well as a high hydrogen recovery through the membranes with the production of pure hydrogen, have been reported [3]. Unfortunately, very few works have focused on the long-term stability of the system and durability of the membranes, which is an important aspect for the Pd-based membrane reactors to become a viable technology.

The stability of membranes in steam reforming was studied in the work of Uemiya et al. published in 1991 [4]. Hydrogen production with a steam reforming Pd membrane reactor was investigated and a constant permeation for at least 10 h was reported, whereas in previous works a decrease in the permeation was reported because of the formation of carbon on the membrane [5–7]. Other works also reported a decrease in the hydrogen permeation, also under non-reactive conditions, i.e., when using either pure hydrogen or hydrogen/nitrogen gas mixtures. Okazaki et al. reported a decrease in the hydrogen permeation above 600 °C due to the strong interaction between the alumina support and the Pd-layer [8]. Fernandez et al. observed a strong interaction also between the TiO_2 support of a catalyst and the Pd-membrane [9]. The works of Okazaki and Fernandez clearly indicate that the materials that come into contact with the membrane should be carefully selected.

Since the flux increases with a decrease in the membrane layer thickness, membrane research has focused on producing thinner layers. For self-supported membranes this has resulted in a reduction of mechanical stability. Recent work of Peters et al. has shown that even 200 µm wide channels do not provide sufficient mechanical support to the membrane to withstand the desired high pressure differences; a 12.5 µm palladium-silver layer deformed over time at 550 °C and 6 bar and started to form cracks reducing the perm-selectivity of the membrane [10]. Supported membranes have the advantage of maintaining high mechanical stability for a very thin membrane layer. Metallic and ceramic supported Pd-based membranes have been prepared by various methods yielding a wide range of permeances and perm-selectivities [3].

In Table 1, a summary of membrane reformer tests that reported the duration and results regarding the stability of the membranes is presented. In most of the works published, a decreased perm-selectivity or deterioration of the membrane performance was reported. However, also a wide variety of causes is reported. A quantitative and better understanding of the rates and causes of the membrane instability and decrease in the perm-selectivity and hydrogen flux will help to manufacture better membranes, as well as improving the design of membrane reactors.

This work investigates the stability of Pd-Ag thin-film membranes on ceramic supports for their application in a fluidized bed membrane reactor. The long-term stability of the Pd-Ag membranes was measured for up to 2750 h at 550 °C. These results were used as a reference to study the stability of the membrane sealing, as well as the contribution of the formation of leakages at high temperatures up to 600 °C and under fluidization conditions.

Table 1. Stability results in literature for membrane reformers.

Reactor Configuration	Feed	Membrane	Membrane Thickness (μm)	Temperature (°C)	Pressure (bar)	Time (h)	Stability Results	H$_2$ Purity (%)	Source
PB	CH$_4$	Pd glass support	20	350−500	1–9	10	• Stable • Previous works had carbon on membrane.	-	[4]
PB	Ethanol	Pd and PdCu	1.3 and 2	280–360	1	45	• Decrease in permeance in first 20 h. • Pinholes and carbon on the Pd membr. After the test (SEM) • Few openings after the test (SEM). • Both membranes retained bulk integrity.	100	[7]
PB	methanol	Pd/Al$_2$O$_3$	~7	280–330	1.5–2.5	1000	• Decrease in ideal perm selectivity 6000 to 4300 (H$_2$/N$_2$)	~100	[11]
PB	Methanol	Pd (support not specified)	24.3	200–300	1–3.44	36	• Deteriorated membrane surface, may be attributed to hydrogen embrittlement. • Visible carbon deposition.	-	[6]
PB	CH$_4$	PdRu (PSS/YSZ)	5	~580	29	1000	• Stable CH$_4$ conversion • Relatively stable H$_2$ recovery • Decline in H$_2$ purity • 20% reduction of H$_2$ flux due to coking. • Nitrogen leak increased two orders of magnitude. • Defects over the entire surface.	>93	[12]
PB	CH$_4$/CO$_2$	Pd/Al$_2$O$_3$	~10	380–450	2.5–3.5	1000	• Decrease in ideal perm selectivity 4300–1000 (H2/N2). • Formation of pinholes and sintering on the membrane • Catalyst deactivation.	96–70	[13]
PB	CH$_4$	Pd/Al$_2$O$_3$	~3.8	580	28	1100	• Carbon formation found on catalyst. • Increase of leak flow • Membrane selectivity decreased 18 times	92–86	[14]
PB	NG	Pd stainless steel supported	20	495–540	9	3310	• Replacement of membranes was required after 492 hours due to leakages. • After replacement H$_2$ purity remained >99.99% • Increase of impurities after 2100 hours.	>99.99	[15]
FB	CH$_4$	PdAg (Inconel)	3 + 1.5 out + in	500–630	2.0–5.3	260	• Overall properties of the membrane were not altered.	-	[16]
FB	EtOH	PdAg/Al$_2$O$_3$	~3–4	450–550	2–4	50	• Test stopped due to failure on sealing.	-	[17]

2. Materials and Methods

2.1. Membrane Preparation

The membranes investigated in this study are thin-film palladium/silver membranes prepared by electroless plating on 100 nm asymmetric Al_2O_3 tubular supports provided by Rauschert Kloster Veilsdorf. Different support dimensions were used, as shown in Figure 1, in particular 10/4 mm and 14/7 mm outer/inner diameter (OD/ID). These supports were used in two different configurations, viz. with both sides open and with one side closed (referred to as "finger-like" supports). The finger-like shape is also porous and covered by the palladium/silver selective layer. Ceramic substrates were activated by immersion into a palladium acetate solution with a subsequent co-deposition of a Pd-Ag layer following the method by Pacheco Tanaka et al. [18]. The palladium concentration was modified according to the dimensions of the supports and the electroless plating process was carried out for 5 h for each membrane. Only membrane 5 (shown in Table 2) had 6 h of deposition. Palladium silver compositions were calculated after analysis of the samples taken from the ELP solution. The results of the characterization carried out by ICP-OES are summarized in Table 2. After the plating step, the metallic layer was annealed at 550 °C for 4 h in a reducing atmosphere (10% H_2 and 90% N_2).

Table 2. Membranes used in this study with electroless plating time and solution composition.

Membrane	ELP Time (h)	Pd%	Ag%
1	5	94.7	5.3
2	5	94.8	5.2
3	5	95.1	4.9
4	5	95.1	4.9
5	6	92.4	7.6

The membranes were sized and sealed using the Swagelok sealing method developed by Fernandez et al. for 10/7 mm outer/inner diameter (OD/ID) [9] as also applied in other studies ([17,19] for 10/4 and 14/7 mm supports respectively).


Figure 1. Sealed membranes with a cross-section; from left to right: A 14/7 mm outer/inner diameter (OD/ID) membrane, a 10/4 mm OD/ID membrane and a 14/7 mm OD/ID finger-like membrane.

2.2. Permeation Modules

Three module configurations were used to study the stability of the membranes (Figure 2), using the same feed and outlet control and analysis systems (one module per time can be used in the permeation setup). The feeding of hydrogen, nitrogen and air (or a mixture of them) was controlled by Bronkhorst mass flow controllers. Membrane module configuration A allows testing of five membranes at once in a single permeation module; this ensured that all the membranes were exposed to exactly the same conditions. The permeate of each of the five membranes can be measured individually. Configuration B is a permeation module where a single membrane was tested. This same module allows for the integration of the membrane in a fluidized bed, as shown in configuration C; the fluidized bed material consisted of Rh/Al_2O_3 particles with an average particle size of 180 μm. The pressure in the system was controlled using a backpressure regulator. The permeate flow rate from the membrane was measured using a Horiba VP film flow meters. For the hydrogen flux the Horiba VP-4 (1–10 L min^{-1}) was used, whereas for the nitrogen flux the Horiba VP-1 was used (0.2–10 mL min^{-1}). In some cases, the nitrogen flow rate was below 0.2 mL min^{-1}, in which case the flux (for the calculation of the perm-selectivity) was set at 0.2 mL min^{-1} with the indication that the actual flux is smaller than this value. Each experimental point is an average of three measurements within an error of 1%.
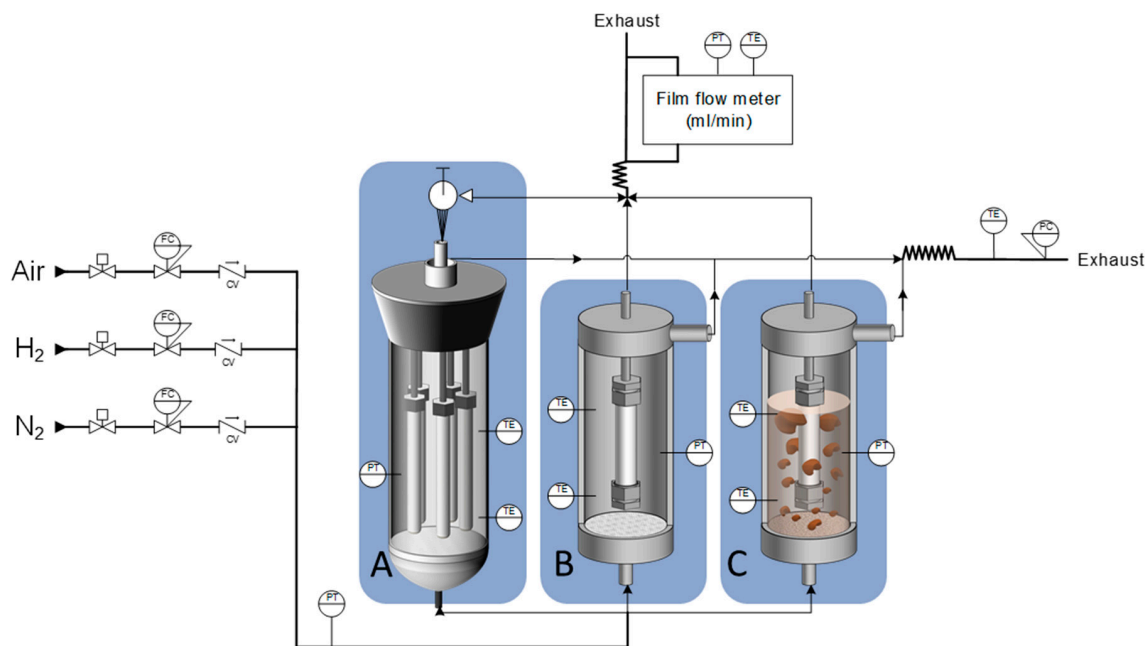
Figure 2. Schematic representation of the permeation modules used in this study.

2.3. Long-Term Stability Tests

The stability of five membranes was studied using configuration A. Membranes 1 and 2 prepared on 14/7 (OD/ID) supports were cut in two parts (indicated with 1a, 1b and 2a, 2b respectively) in order to investigate the stability evolution of two equally prepared membranes. Membrane 2a had a finger-like part; this membrane was used to investigate the effect of the membrane sealing on the stability. Membrane 3 was prepared on a 10/4 support, and due to the lower thickness of the support, a lower torque was applied to seal this membrane. The five membranes were in total operated for 2000 h. After 2000 h, membrane 1a and 2a were removed for intermediate characterization, while the other membranes were operated for another 750 h. Membrane number 4 (10/4 OD/ID) was studied as a single membrane at high temperature. The membrane was stabilized at 400 °C for 150 h and operated at 550 °C and 600 °C. Membrane 4b and 5, were both: Finger-like, 10/4 (OD/ID), 265 mm long and sealed with the same torque. These membranes were used to study the influence of the

fluidization on the permeation properties. The membranes were integrated into two separate reactors and stabilized at 400 °C for 150 h. After this period, a catalyst bed was introduced into the reactor containing membrane 4b. The minimum fluidization velocity was experimentally determined with the standard pressure-drop method to ensure the fluidization velocity was set at 3 times the minimum fluidization velocity. Both membranes were first kept at 400 °C and after 700 h the temperature was increased to 500 °C. The gas feed was a 50:50 mixture of nitrogen and hydrogen, the nitrogen ensured that the permeation of hydrogen did not decrease the fluidization velocity too much so that the velocity was kept well above the minimum fluidization velocity (although this induced external mass transfer limitations, which are not relevant for this study of membrane stability and are not further discussed in this study). The membrane parts and experimental details are summarized in Table 3.

Table 3. Details of membranes and conditions used in this work.

Membrane Number	Reactor Configuration	Support Material	Size Ø Outer/Inner (mm)	Sealing Top	Bottom	Length (mm)	Temperature (°C)	Time Tested (h)	On Stream [1]
1a	5 membranes Empty tube	Pd-Ag Al_2O_3 100 nm	14/7	Swagelok 12 Nm	Swagelok 12 Nm	105	400–525	2000	H^2
1b	5 membranes Empty tube	Pd-Ag Al_2O_3 100 nm	14/7	Swagelok 12 Nm	Swagelok 12 Nm	90.5	400–550	2650	H^2
2a	5 membranes Empty tube	Pd-Ag Al_2O_3 100 nm	14/7	Swagelok 12 Nm	Finger-like	112	400–525	2000	H^2
2b	5 membranes Empty tube	Pd-Ag Al_2O_3 100 nm	14/7	Swagelok 14 Nm	Swagelok 14 Nm	75	400–550	2650	H^2
3	5 membranes Empty tube	Pd-Ag Al_2O_3 100 nm	10/4	Swagelok 7 Nm	Swagelok 7 Nm	107.5	400–550	2650	H^2
4a	Single membrane Empty tube	Pd-Ag Al_2O_3 100 nm	10/4	Swagelok 6 Nm	Swagelok 6 Nm	87.98	400–600	715	H^2
4b	Single membrane Fluidized bed	Pd-Ag Al_2O_3 100 nm	10/4	Swagelok 6 Nm	Finger-like	265	400–500	1150	H^2/N_2 (50:50)
5	Single membrane Empty tube	Pd-Ag Al_2O_3 100 nm	10/4	Swagelok 6 Nm	Finger-like	265	400–500	1150	H^2/N_2 (50:50)

[1] "On stream" indicates the gas or gas mixture the membranes were exposed to when not being measured.

2.4. Membrane Characterization

After the membranes were tested the systems were cooled down in nitrogen. When at room temperature the nitrogen flux was measured at different pressures and the membranes were removed from the system. The sealing parts were covered with a resin, to distinguish the leakage contribution of the sealing from the leakages from the surface, and subsequently the permeation of nitrogen was again measured (dry permeation). To obtain the pore sizes of the pinholes, capillary flow porometry was used. The membranes were immersed in ethanol and the nitrogen flux as a function of the pressure was measured (wet permeation). With the dry and wet permeation lines, the pore size of the pinholes was estimated using the Young-Laplace equation [20].

2.5. Post Mortem Characterization

After the post characterization, the seals were removed and the membranes were characterized by X-Ray Diffraction (XRD), Scanning Electron Microscopy (SEM) and Energy Dispersive Spectroscopy (EDS). The XRD analysis was performed at 1.5406 Å, with the Rigaku Miniflex 600. SEM was performed on both a cross-section and the surface of the membranes, using secondary electrons and backscattered electrons, with a Phenom Pro X. The EDS was performed on the same system as the SEM at 15 kV.

3. Results and Discussion

In order to integrate the membranes in the reactors, each membrane was connected to a dense metallic tube using Swagelok and graphite seals. The mechanical stress that can be induced on the membranes by the Swagelok sealing method is found to be limited by the support and could result in failure of the membrane sealing during operation. The 10/4 supports used in this work allow for sealing with a higher torque than used on the 10/7 mm OD/ID membranes presented in the work of Fernandez et al [9]. However, Spallina et al. used also 10/4 supports and reported significant failure of the membranes [17]. For the sealing of the membranes in this work it was found that the torque applied on the 10/4 supports could be increased compared to the 10/7 membranes. The 14/7 mm OD/ID support was found to withstand a sealing torque exceeding 20 Nm. However, at this torque level the membrane showed damage to the thin palladium film, therefore the maximum torque applied in this work was set to 14 Nm. All membranes investigated in this work were leak tested prior to other tests. The quality of the sealing can be considered as a potential contribution to the decrease in perm-selectivity of the membranes. Thus, a reduction in the number of sealing points could improve the stability of the membrane. In this work finger-like membranes were used where the end cap of the membrane is completely covered with the palladium layer. The end cap is made of a porous ceramic part formed during the support production and therefore also contributing to the total surface area of the membrane [21].

3.1. Air Treatment and Initial Conditions

Air treatment is usually performed to stabilize and increase the hydrogen flux [22–24]. Roa et al. have shown that the air treatment had more than a cleaning effect on the surface of the membranes and also caused morphological changes of the surface [25]. However, it has been reported that air treatment also increased the nitrogen flux indicating the formation of pinholes. The membranes in this work were heated up to the desired temperatures under nitrogen; at this temperature, the nitrogen permeation was measured followed by an air treatment. The air treatment was performed by flushing a 50:50 air/nitrogen mixture into the system for 2 minutes; for membranes 1a, 1b, 2a, 2b and 3 at 500 °C, and for membranes 4a, 4b and 5 at 400 °C respectively. After the treatment, the nitrogen and hydrogen flux were measured again. The obtained permeation results are reported in Figure 3.
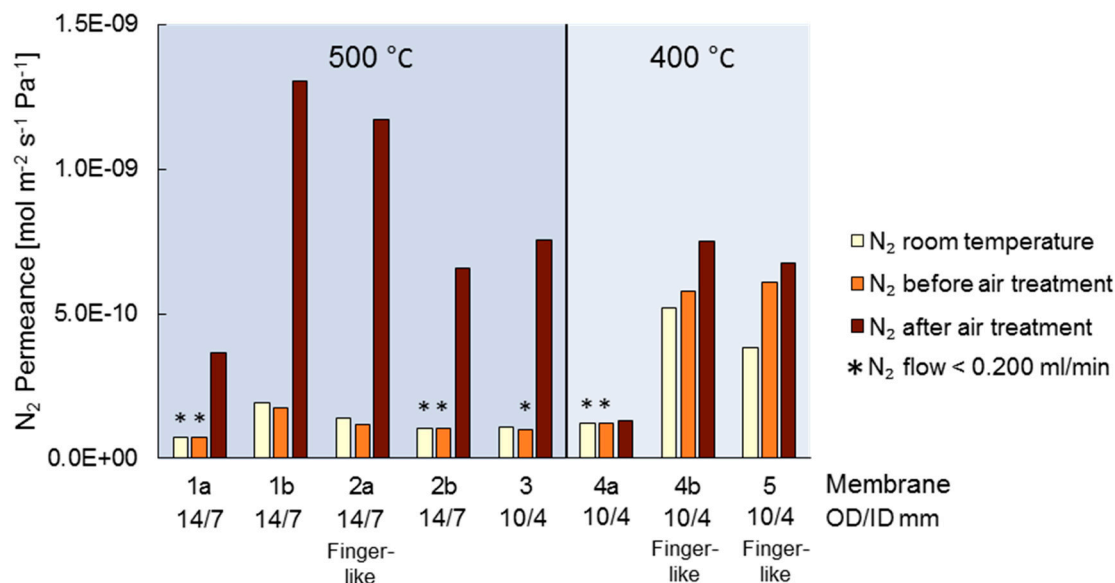
Figure 3. Nitrogen permeance before and after heating and air treatment.

The results show that the nitrogen permeance after the air treatment increases between 400% and 700% at 500 °C, which is significantly more than 10% to 30% at 400 °C. The increase in nitrogen permeance could be the result of a rearrangement of the palladium surface because of oxidation, which may cause defects. The formation and connection of defects through the palladium layer as a result of this rearrangement could subsequently result in the formation of pinholes. The results show that this effect is more pronounced at higher temperatures. This can be related to the higher reaction kinetics of palladium oxidation at higher temperatures, which results in a faster and less structured rearrangement [26]. The air treatment did not show significantly different effects for the finger-like membrane compared to the other membranes, indicating that the graphite ferrules in the sealing are not significantly affected by the air treatment, both at 400 °C and 500 °C. The hydrogen flux increased from 70% up to 110% compared to the case before the air treatment; this is expected and comparable to the increases reported before in the literature [22]. The ideal perm-selectivity ranged, after the air activation, between 7500 and 9000 at 500 °C for these membranes. In Appendix A the ideal perm-selectivity of all the membranes at different times in this study is presented. The results of the permeation test for all the membranes at their initial conditions are shown in Figure 4. The permeation flux of all membranes after activation showed good correspondence with the transmembrane difference of the square root of the hydrogen partial pressure, indicating that the hydrogen flux is only limited by bulk diffusion of hydrogen in the palladium layer. Both parts of membrane 1 and 2 showed almost the same hydrogen permeance, whereas the permeance of membrane number 3 was found to be 1.2 times higher than that of membrane 1 and 2. We can relate this difference to a minor difference in the (thickness of the) selective layer and not to differences in the dimensions of the support, since the pressure exponent showed a good fit with 0.5 for all membranes, indicating no effect of the support. Membrane 4 showed a higher permeance compared to membrane 5, which can be explained by the longer time of the ELP process of membrane 5 which was expected to result in a slightly thicker Pd-Ag layer, lowering the hydrogen permeance.
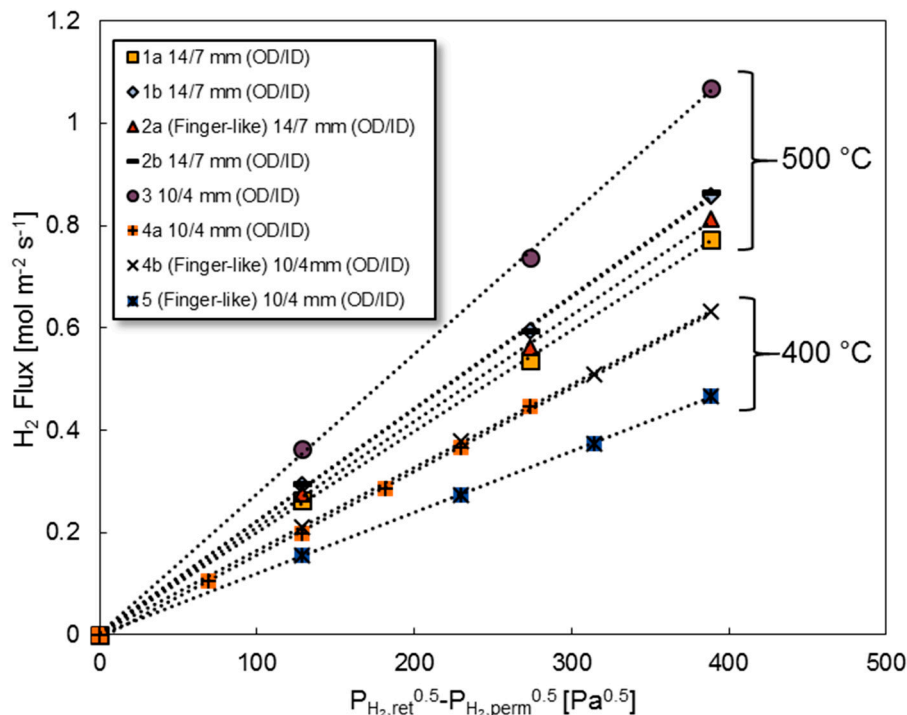
Figure 4. Initial hydrogen permeance of the membranes as measured after air activation.

3.2. Long-Term Stability

Membranes 1a, 1b, 2a, 2b and 3 were studied to compare the different seals and sealing forces. The long-term behaviour of these membranes was investigated at 500 °C, 525 °C and 550 °C using setup configuration A. Both the hydrogen and nitrogen permeances are measured over the tested time, and are shown in Figure 5a,b, respectively. The hydrogen permeance initially increased, however after 200 h it stabilized for membranes 1a, 1b, 2a and 2b. This process was shown to be faster for membrane 3. This initial increase is understood as a period of further annealing of the membrane. The duration of this period is therefore dependent on the initial conditions of the membrane (concentration and phases present on the membrane layer), which is the cause of the difference in stabilization period between the membranes. The initial conditions of the membrane are further investigated during the post mortem characterization. After this initial increase the hydrogen permeance decreased for all the membranes, however, for membrane 3 it decreased more significantly. The hydrogen permeance stabilized after ca. 1000 h. At this point the temperature was increased to 525 °C, and an increase in the hydrogen permeability as a result of the increased temperature is observed. This is followed with a similar initial increase over time as seen at 500 °C followed by a decrease, which then again stabilizes. Once again, for membrane 3 the process is more pronounced and faster. After 2000 h on stream, the system was cooled down and membrane 1a and 2a were removed. After heating up the system, the remaining membranes showed stable hydrogen permeance. Following the stable period, the system was heated further to 550 °C. At this temperature a direct decrease in the hydrogen permeance was measured. After 2750 h the test was stopped in order to analyse the membranes. The effects of the high operating temperature of 550 °C and above are further investigated using membrane 4a.
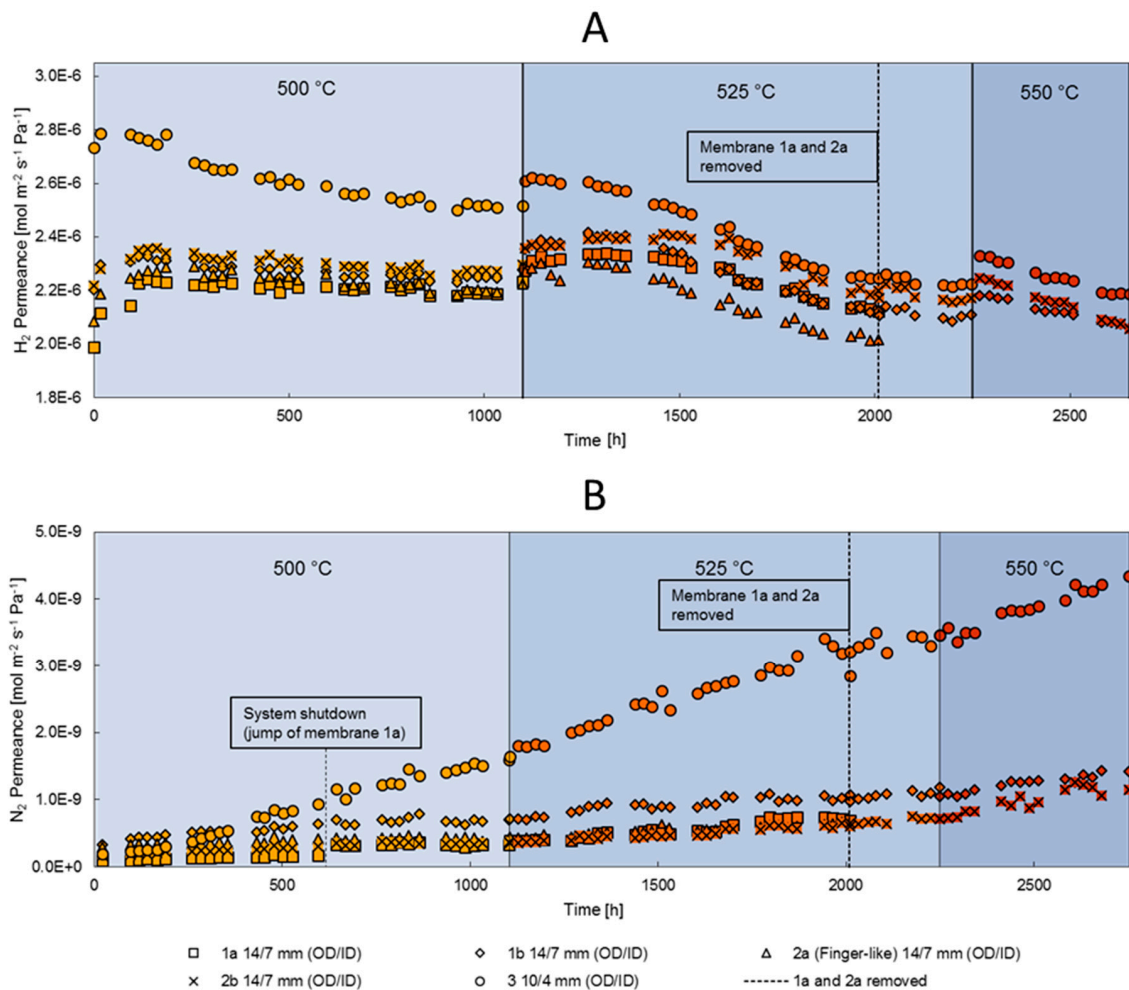
Figure 5. Long-term hydrogen permeance (**A**) and nitrogen permeance (**B**) of membranes 1a, 1b, 2a, 2b and 3 at 500 °C, 525 °C and 550 °C.

The increase in nitrogen permeation follows a linear trend over time for all the membranes. However, membrane 3 shows a more pronounced increase in nitrogen permeance. Due to a shutdown of the system (at around 600 hr), membrane 1a made a small jump up in nitrogen permeance. The other membranes seemed to be unaffected by this shutdown. The ideal perm-selectivity ranged after the long-term test from 755 to 3100 at 550 °C for membrane 1b, 2b and 3.

To further compare the long-term behaviour of the membranes both the time derivative of the hydrogen and nitrogen permeance were calculated and compared for each temperature (see Figure 6). In the calculations of the slopes the initial increase was not considered for the hydrogen permeation. The hydrogen permeance has a negative slope as the permeation decreases over time; it is clear that the slopes become more significant at higher temperatures. The decrease in hydrogen permeability is possibly related to surface deformation, of which the rate is increased at higher temperatures [27]. The surface transformations are further investigated in the post characterization.
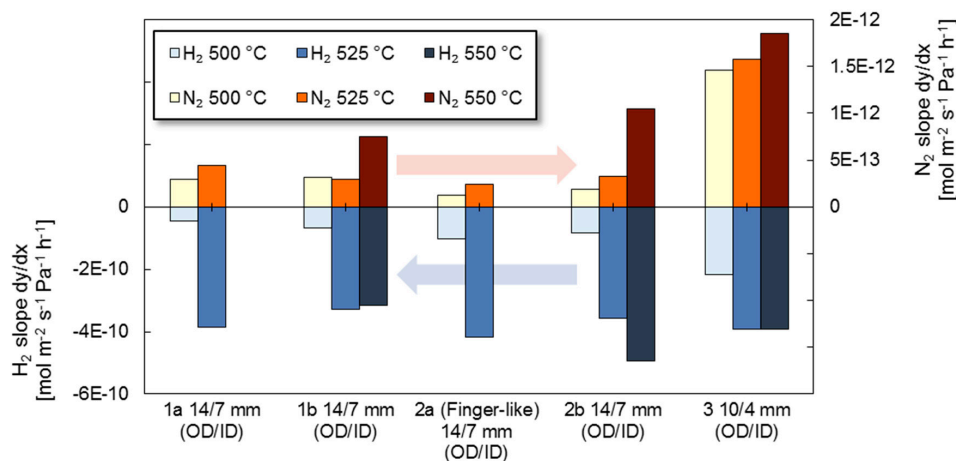
Figure 6. Slope of hydrogen and nitrogen permeance over time.

The slopes of the nitrogen permeance of the tested membranes are relatively small compared to literature. Abu El Hawa reported slopes of 4×10^{-11} down to 5×10^{-12} mol m^{-2} s^{-1} Pa^{-1} h^{-1} for metallic supported membranes with a 30 μm layer of YSZ [28]. With an increase of the temperature the slope of the nitrogen permeance increases almost for all the membranes. Membrane 2a (finger-like) shows the lowest increase in nitrogen permeation due to the fact that this membrane has only one sealing. To further investigate this, the relative nitrogen permeance was determined by dividing the nitrogen permeance by the initial nitrogen permeance, which is shown in Figure 7. These results show that the relative nitrogen permeance of membrane 2a is half that of membrane 2b (which was originally part of the same membrane, but has now two sealings), also membrane 1a shows that the relative nitrogen permeance is doubled compared to membrane 1b. This indicates that the main contribution of the nitrogen permeance increase over time is related to the sealing. Thus, also the larger increase in nitrogen permeance through membrane 3 can be suspected to be caused by the lower force applied to the sealing. At 525 °C this effect was less pronounced, which could indicate an increased contribution of leakages through pinholes formed on the surface. If the surface contribution increases the effect of the sealings become less pronounced.
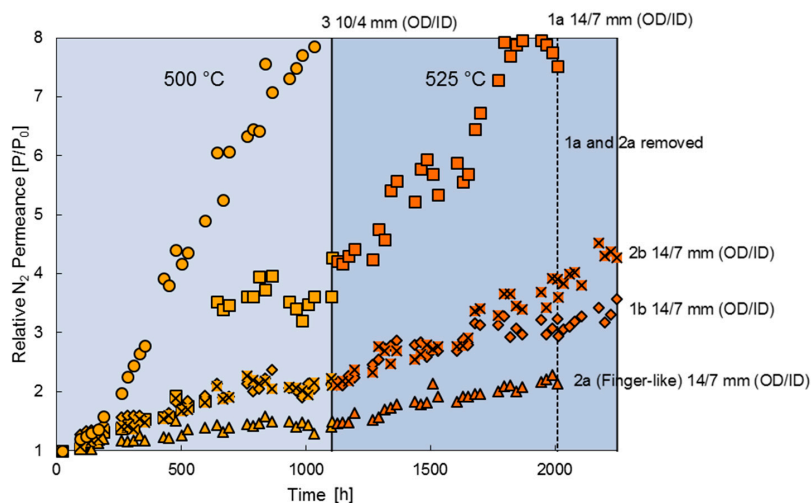

Figure 7. Relative nitrogen permeance of the membranes 1a to 3 in the long-term membrane test.

3.3. High Temperature Stability

To investigate the membrane stability at temperatures above 550 °C membrane 4a was used, as shown in Figure 8. The hydrogen permeance increases with temperature; at 500 °C this increase is more pronounced due to the stabilization of the Pd-Ag layer; the corresponding nitrogen permeance,

as well as the slope of nitrogen permeance are comparable to those observed for membrane 3 at both 500 °C and 550 °C. At 600 °C there is a very large decrease in the hydrogen permeance and a very pronounced increase in nitrogen permeance, which eventually resulted in membrane failure (i.e., ideal perm-selectivity <500). The decrease in hydrogen flux was expected, since at 600 °C there is a strong interaction between the alumina support and the palladium layer [8]. A similar increase in nitrogen permeation was observed after 150 h at 600 °C in single gas conditions for a $Pd_{94.9}Ag_{5.1}$ membrane by Melendez et al. [29]. The main purpose of the high temperature stability test in this work is to differentiate between different effects that cause the increase in nitrogen permeance, which is further discussed in the post characterization section.
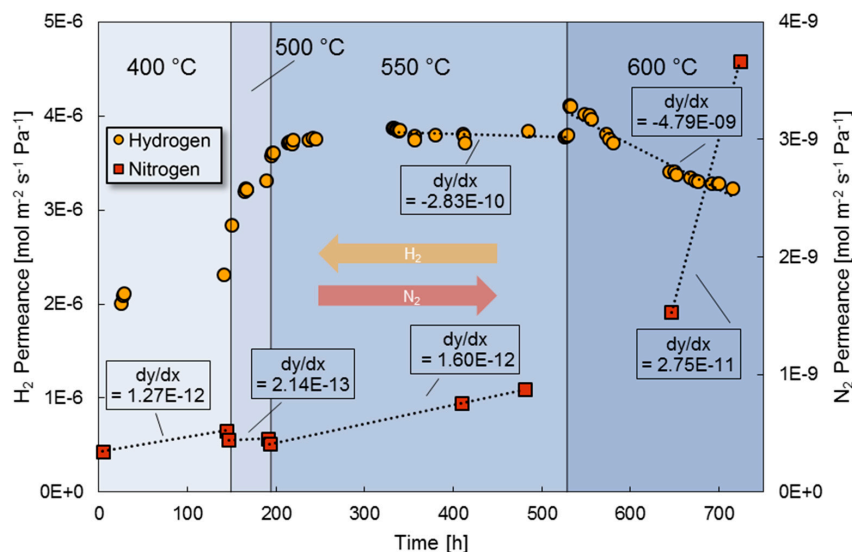

Figure 8. Effect of temperature on the long-term hydrogen and nitrogen permeance of membrane 4a.

3.4. Fluidization Bed Conditions

In order to study the effect of fluidization on the hydrogen and nitrogen permeation, two similar finger-like membranes, 4b and 5, were integrated into two identical reactors and the nitrogen and hydrogen permeances were measured. Both membranes were activated with an air treatment and were subsequently stabilized at 400 °C. Both membranes showed similar performance and stability, as can be seen from Figure 9a,b showing the hydrogen and nitrogen permeance respectively. Membrane 4b exhibited a somewhat higher initial hydrogen permeance, whereas nitrogen permeance for both membranes was similar. After the stabilization period the systems were cooled, the catalyst bed was introduced into the system of membrane 4b and both systems were heated back up. After heating up, membrane 4b showed a small step increase in the hydrogen permeance, whereas membrane 5 showed a step decrease; the increase in hydrogen permeance of membrane 4b could be explained by a higher average temperature in the system; the temperature profile along membrane 4b in the fluidized bed became more uniform and hence a higher permeation was obtained. The step decrease can be related to a deactivation of the palladium layer during the cool-down cycle, however this behaviour is normally not observed for these membranes when cooled down and heated back up. Nitrogen permeation is also affected by the cool-down and the integration of the catalyst. During fluidization, membrane 4b showed a decrease in the hydrogen permeance during the first 250 h, after which, stable hydrogen permeance was obtained. The nitrogen permeance of membrane 4b decreased under fluidization, in contrast to all other experiments. It is suspected that both effects are the result of catalyst particles covering the membrane surface, covering the pinholes and reducing the surface area available for hydrogen adsorption. Membrane 5 exhibited stable hydrogen and nitrogen permeance over this period. After 850 h the system temperatures were increased to 500 °C. Both membranes showed an increased hydrogen permeance related to this temperature increase. Membrane 5 showed initially

a decrease in the hydrogen permeance, which could be attributed to the change in temperature distribution along the membrane. Nevertheless, the temperature along membrane 4b in the fluidized bed was found to be stable and still an increase in the hydrogen permeance was observed. Taking the nitrogen permeance into account, stable operation for membrane 5 was observed, whereas a large increase in nitrogen permeance was observed for membrane 4b. From these results it can be concluded that the membrane and sealing was significantly affected by the presence of the fluidized bed at 500 °C. To investigate whether the extent of the leakages increases gradually with higher operating temperature, or whether there is a strong increase at a certain temperature, membrane 5 was resealed after post characterization, placed in the fluidized bed and then tested again at 450 °C and 500 °C under the same conditions as for membrane 4b before (results are not shown in the figure, since the time scales were shorter). The nitrogen slope at 450 °C was found to be 4.8×10^{-13} mol m^{-2} s^{-1} Pa^{-1} h^{-1} and at 500 °C 1.5×10^{-11} mol m^{-2} s^{-1} Pa^{-1} h^{-1}. The nitrogen permeation increased with a factor 3 between 400 °C and 450 °C, while it increased with a factor 31 when going from 450 °C to 500 °C. These results suggest a critical change between 450 °C and 500 °C, where the leak rate increases significantly. Post characterization of the membranes was performed in order to understand the main contribution to membrane failure.
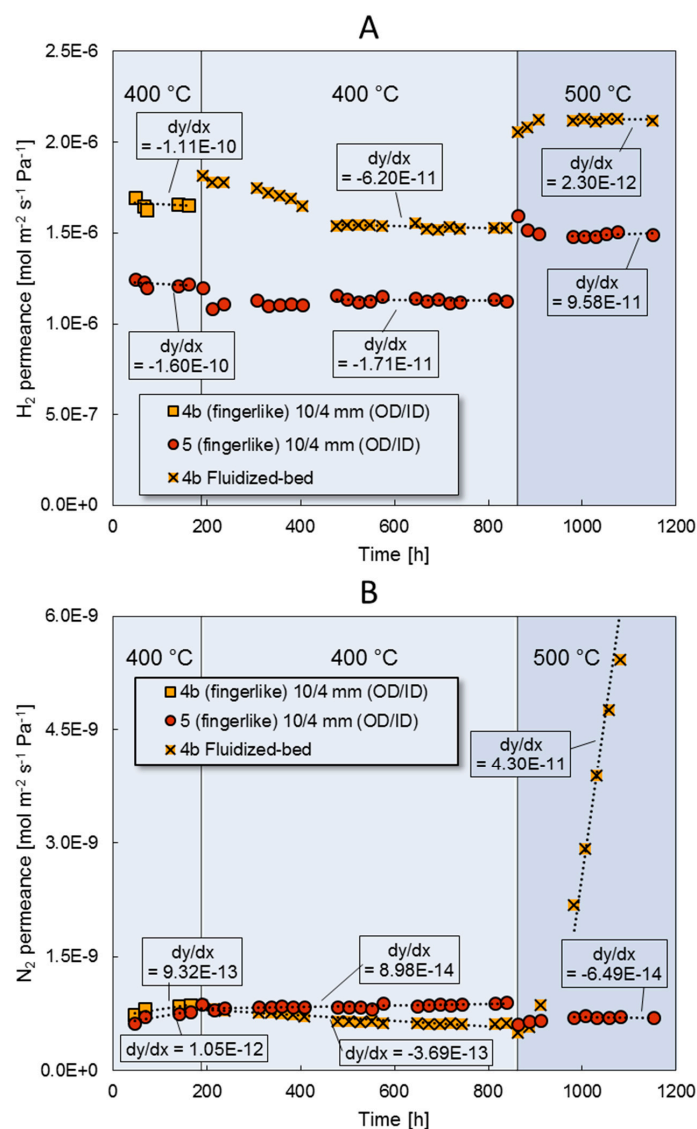
Figure 9. Hydrogen permeance (**A**) and nitrogen permeance (**B**) of membrane 4b in the fluidized bed and membrane 5 in the empty system.

3.5. Post Characterization

To better understand the origin of the increase in nitrogen permeance of the tested membranes, capillary flow porometry was used (after closing the sealing parts by using a gas tight resin). The results of the capillary flow porometry are translated to pore sizes using the Young-Laplace equation; the results are shown in Figure 10. The pore distribution for membrane 4a could not be determined due to damage to the membrane while preparing the sample.
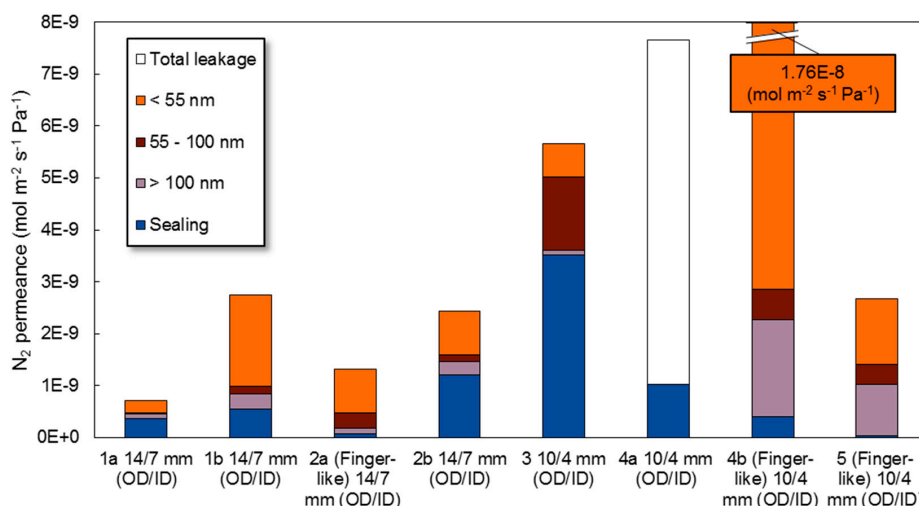
Figure 10. Nitrogen permeance contributions at room temperature, with corresponding pore size contributions.

The blue part in the bars in Figure 10 shows which part was a result of leakages from the sealing. It is clear from the figure that the contribution of leakages from the sealing was the lowest for finger-like membranes 2a, 4b and 5 with only one sealing, which confirms the results obtained during the long-term stability tests that the sealing contributes partly to the nitrogen permeance and can be decreased by decreasing the number of sealings used. Moreover, it can be seen that the contribution of the sealing to the nitrogen permeance on membrane 3 was significantly higher because of the lower torque applied on the sealing. However, the increase in nitrogen permeation during the long-term stability test could also be related to the formation of large pores, as they show to have a significant contribution to the overall leakage rate as well. In membranes 1a, 1b, 2a and 2b most of the contribution is shown to result from pores with a size smaller than 55 nm. Membrane 4b and 5 show a large contribution of pores larger than 100 nm and pores smaller than 55 nm. The contribution of the large pores was expected for membranes 4b and 5 since minor pinholes were visible on the surface when the membranes were immersed in ethanol before the high temperature tests were carried out.

The different contributions to the nitrogen permeance of membranes 4b and 5 were studied in more detail to investigate whether the finger-like part of the membrane 4b suffered more damage from the fluidization than other parts of the membrane. To this end, the membranes were immersed in increments of 1 cm in ethanol while the permeate side was pressurized with helium from the inside of the membrane. The helium flow rate was measured during the immersion. The pressure difference over the membrane was selected such that the ethanol closed all the pinholes during the test and that no bubbles were observed from the membrane surface.

Figure 11 shows the distribution of the leakage rates along the membrane, where the relative-length 0.0 represents the tip of the finger-like membrane. From these results it can be observed that membrane 5 shows a relatively equal distribution along its length with some parts that show a slightly larger contribution with more pinholes. Peters et al. reported also an almost evenly distribution of the leaks for Pd membranes [30]. Membrane 4b which was in the fluidized bed showed a higher total helium flow rate; however, no significantly higher contribution is obtained from the finger-like

part, suggesting that the finger-like part did not suffer more than the other parts in the fluidized bed. For membrane 4b the helium flow rate along the membrane increased with the length of the membrane. It is suspected that this is related to interactions of the catalyst particles and the Pd film in the fluidized bed reactor. An inherent property of a fluidized bed is that bubbles of gas rise through the bed of solid particles, the size of the bubbles grow along the reactor. These bubbles carry particles in their wake inducing a solids circulation [31]. As bubbles rise in the bed, they grow and rise with higher velocity, thereby also increasing the particle velocity. The higher particle velocity results in the increased energy of impact of the collisions of the particles on the membrane. The results suggest that the increase in leakage rate is related to the increase in the mechanical impact of the fluidized bed on the membranes. The temperature plays in this case a detrimental role in when the collisions of the particles become destructive to the membrane.
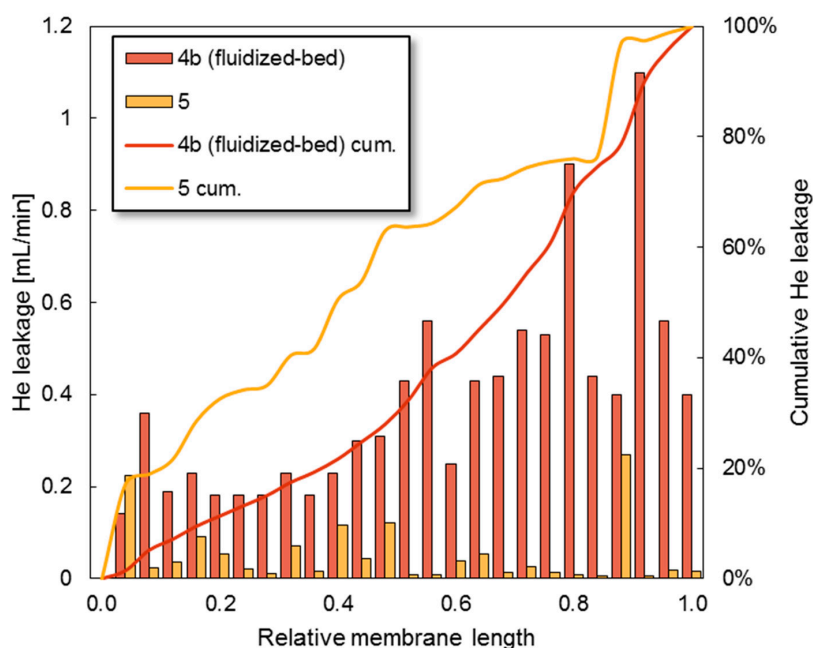

Figure 11. Helium flow rate distribution along the membrane 4b and 5.

### 3.6. Post Mortem Characterization

3.6.1. XRD

To verify whether there is chemical interaction and to investigate the alloying condition, XRD analysis has been used. Samples of the pre-tested membranes were compared with samples of the membranes after the tests. The results of the XRD analysis are presented in Figure 12. The only peaks that are distinguished correspond to either Pd, Ag or the alloy of $Pd_{75}Ag_{25}$. The pre-testing sample showed for membranes 1, 2 and 4 a split in the peak indicating that the alloy of Pd-Ag is not completely formed yet during the alloying after preparation. The difference in required alloying time is most likely a result of differences in the co-deposition during the ELP. This alloying can explain the increase in the hydrogen permeance during the first 200 hours of membranes 1 and 2 as opposed to membrane 3 in the long-term test [27]. The intensity of the used membrane 1, 2 and 3 are 2 to 3 times larger compared to the fresh membrane samples. The differences in the peak width and intensity indicate a change in morphology. According to the Scherrer Equation (1), the crystal size is inversely proportional to the peak width. In Table 4, the following crystal sizes were obtained for the tested membranes applying the Scherrer equation:

$$B = \frac{K\lambda}{Lcos(\theta)}, \tag{1}$$

Membranes 1, 2 and 3 show significant crystal growth with increased time on stream and temperature. The growth of crystals can be related to the growth in grain size. The growth of the grains can be used to explain the reduction in the hydrogen flux for membrane 1, 2 and 3. The diffusion of hydrogen along the grain boundary is ~100 times faster than the diffusion through the lattice [32]. The grain growth reduces the grain boundary density, hence the decrease in hydrogen flux [33]. SEM analysis was performed to confirm the grain growth and further investigate the structural changes.

Table 4. Crystal sizes calculated from XRD results.

| Membrane		Peak 111	Peak 200
		Crystal Size (nm)	Crystal Size (nm)
1	Pre testing	44	34
1a	used 2000 h	59	41
1b	used 2650 h	72	54
2	Pre testing	59	53
2a	used 2000 h	64	41
2b	used 2650 h	64	46
3	Pre testing	44	46
	used 2650 h	72	54
4	Pre testing	17	11
4a	after 715 h (600 °C)	64	51
4b	after FB 1150 h (500 °C)	64	48
5	Pre testing	61	46
	used 1150 h (500 °C)	59	48
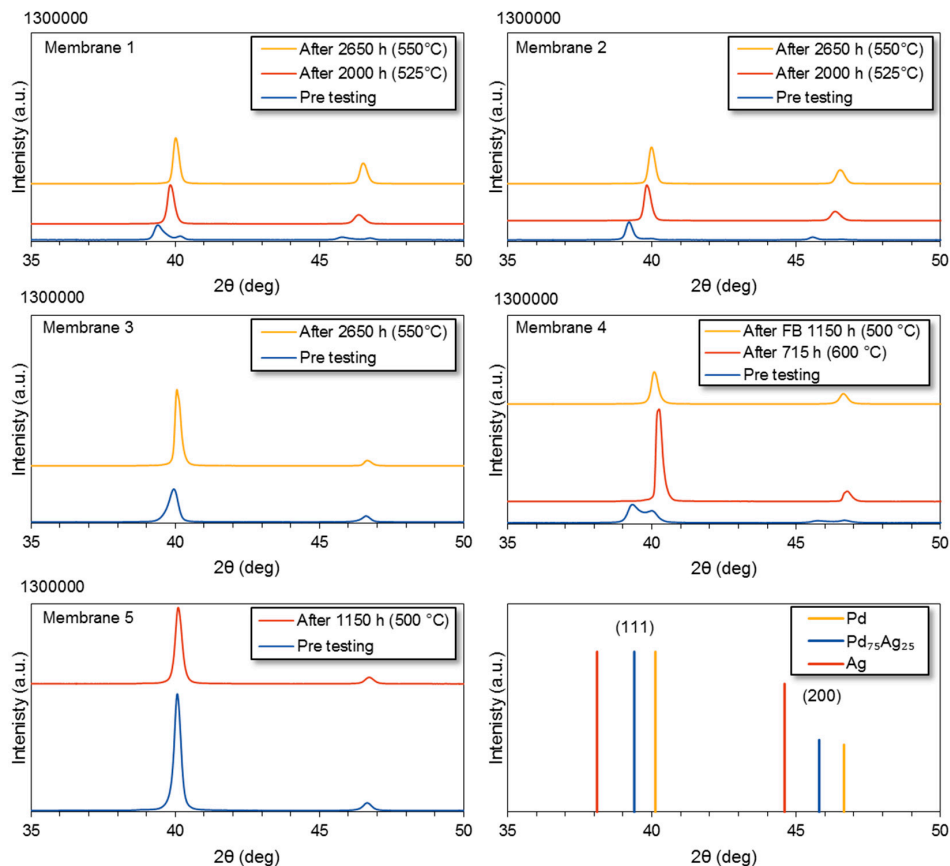
Figure 12. XRD profiles of the different membranes before and after testing.

3.6.2. SEM Analysis

SEM analysis is used to further investigate the changes in the surface of the selective layers and to measure the thickness of the membranes, pre and post testing. Figure 13 shows the evolution of the surface of membrane 1 during the long-term test. Prior to the test, a smooth surface with a very small grain size can be observed. After 2000 h of operation and a temperature up to 525 °C the grain size is increased, which even further increases after 2650 h up to 550 °C. As can be seen, the grain boundary density is decreased and, as mentioned before, this can explain the observed decrease in the hydrogen flux. Besides the formation of larger grains, the membranes showed the formation of small pinholes. The formation of pinholes was relatively pronounced for membrane 3, where some of the black spots appear to be holes between the grain boundaries, as shown in Figure 14A. The sizes of these defects, however, do not directly correspond to the size of the pinholes found by porometry. This would suggest that below the surface there is a narrower pitch between these defects which is measured by the porometry, while the growth and agglomeration of the grains result in the formation of these defects. Figure 14B shows the surface of membrane 4a, where the grains show a wide size distribution and seemed to have grown irregularly. Also from the porometry test it was concluded that the surface of membrane 4a contributes significantly to the nitrogen permeation. Moreover, membranes 1, 2, 3 and 4a showed an increase in crystal growth from the XRD results. Previous works indicated that microstructural changes of the surface result in the formation of void spaces [30,34–36]. It can therefore be suspected that the formation and connection of these defects resulted in the formation of pinholes, and at higher temperatures the more irregular surface deformation increases the number of defects formed and thereby the chance of the formation of pinholes. The thickness of the selective layer was also measured on a cross-section of the membranes. The thickness of the selective layer of membranes 1, 2, 3, 4a and membrane 5 before fluidization showed no changed compared to the fresh sample thickness of 4 to 5 microns. Membrane 5 was expected to have a higher thickness, which could also be expected from the permeation results. However, from the cross-section measured this could not be accurately confirmed.
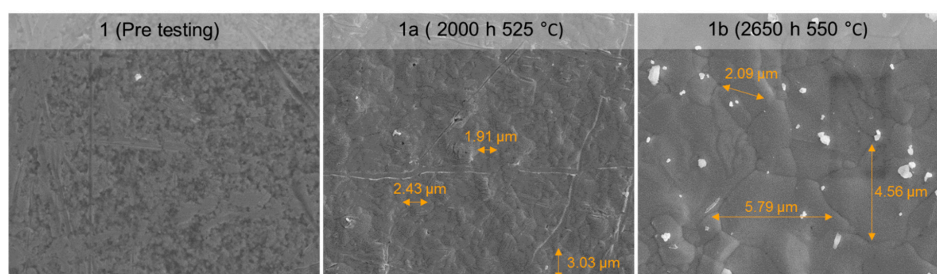

Figure 13. SEM pictures of the surface of membrane 1 pre-testing, after 2000 h and after 2650 h.
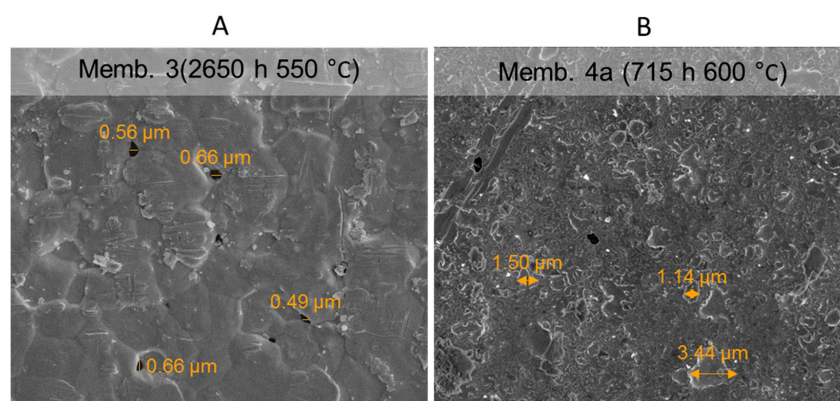

Figure 14. SEM picture of pinholes on the surface of membrane 3 after 2650 h and up to 550 °C (**A**), SEM picture of the surface of membrane 4b after 715 h of operation up to 600 °C (**B**).

Membrane 4b that was operated in the fluidized bed was divided into 3 sections to inspect the change of the surface along the membrane. In Figure 15 the surface of the membrane is shown for the three sections at two different magnifications, with the flow direction being from the bottom to the top of the images. A clear pattern is visible in the flow direction were towards the top the pattern becomes less spikey and more flat. The pattern looks like overlapping grains, like a fish scale. As mentioned in the discussion of the permeation results, the main increase in nitrogen permeation was found to occur between 450 °C and 500 °C. Helmi et al. [37] showed that no significant surface effects were visible after fluidization at 400 °C. Therefore, it is expected that the main surface deformation took place between 450 °C and 500 °C. It is expected that a combination of operation at the temperatures above 450 °C, and the scouring action of the fluidized particles, results in an increase in surface energy. Since the palladium layer is ductile and the hardness of the palladium decreases with temperature, the increased surface energy could allow ductile deformation of the PdAg layer. EDS analyses, as shown in Figure 16, revealed that the pattern formed on the surface is relatively homogeneous in composition indicating more mechanical interactions than chemical interactions with the catalyst. Beside the pattern, the surface itself also shows many small darker spots. From the EDS results in the dark spots a high presence of Al and O was found. Closer inspection showed that the dark spots where mainly holes. The high concentration of Al and O could be explained due to fines of the catalyst that are stuck in the holes of the surface. The thickness was measured with SEM on 4 different points along the membrane, using Figure 15 as a reference, at point A, Between A and B, Between B and C and at point C. The average thickness is shown to decrease from bottom to top with about 1 μm. This decrease in thickness seems to corroborate with the the leak distribution results that showed a larger leakage contribution towards the top of the membrane as a result of the increased particle velocity. This shows that the configuration and design of a system can significantly affect the stability of the membranes, since the hydrodynamics play an important role in the particle velocities. Possible solutions to avoid the erosion effects observed in this work can be found in protecting the membranes with a porous ceramic layer, as presented in the recent work by Arratibel et al. [38].
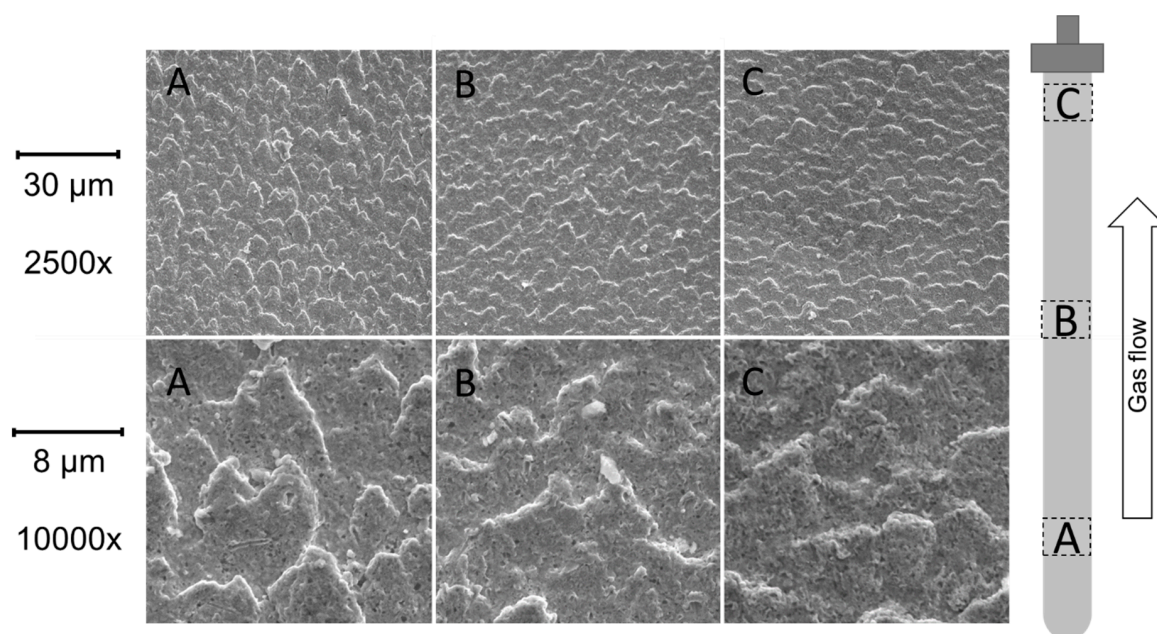
Figure 15. Surface effects on membrane 4b after 1150 h and fluidization up to 500 °C.
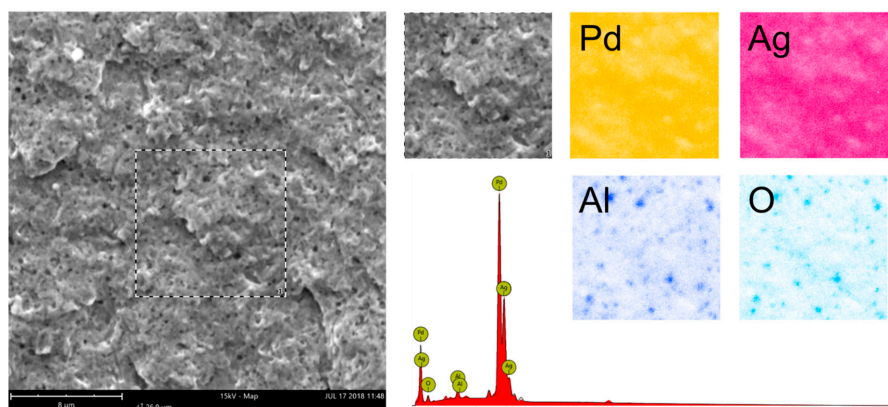
Figure 16. Energy Dispersive Spectroscop (EDS) on membrane 4b section B after 1150 h and fluidization up to 500 °C.

4. Conclusions

In this study has the stability of the performance of thin-film PdAg membranes supported on Al_2O_3 supports over longer times on stream have been investigated, assessing the relative contribution of the sealings and surface defects at different operating temperatures and with or without fluidized catalyst particles. The long-term stability experiments have shown an important contribution of leakages through the sealings, especially at lower operating conditions, where a reduction in the number of sealings resulted in a more stable operation. At temperatures above 500 °C the contribution of leakages from the surface becomes more pronounced and larger than the leakages through the sealings. The leak rates for the different membranes have been reported and can be used as a comparative basis for future works. Post characterization showed that the main leakages originate from small pinholes <55 nm in the surface of the membranes. Small surface defects are formed due to the agglomeration of Pd grains, while the increased grain size decreases the grain boundary density and thus also the hydrogen permeation rate over time. At temperatures above 550 °C a wide distribution of grain sizes on the surface is observed with a high contribution of surface defects. The results of these high-temperature experiments showed that when steam reforming is performed at temperatures above 500 °C a decrease in the perm-selectivity can be expected.

The integration of membranes in a fluidized bed up to 450 °C showed no significant impact on the stability of the palladium membranes. However, between 450 °C and 500 °C the membrane surface is significantly affected and the nitrogen permeance increases rapidly. Post characterization revealed that the bed hydrodynamics play a significant role in the extent of erosion of the membranes in the fluidized bed.

From the observations obtained in this work from both the long-term tests and the tests in the fluidized bed it can be concluded that membrane reactors operated under reforming conditions for hydrogen production require improved membranes in terms of thermal stability. For the integration of the membranes in fluidized bed membrane reactors, the selective layer of PdAg needs to be protected or its mechanical stability needs to be improved, while simultaneously the design of fluidized bed membrane reactors needs to be revisited to further improve the bed hydrodynamics and decrease the scouring action of the particles on the membranes.

Appendix A

Table A1. Ideal H_2/N_2 perm selectivity during the tests for all membranes involved.

Membranes	Ideal H_2/N_2 Perm-Selectivity ΔP 1 bar/Total Time on Tream +- (h)													
	400 °C	400 °C	400 °C	500 °C	500 °C	500 °C	500 °C	525 °C	525 °C	525 °C	550 °C	550 °C	600 °C	600 °C
1a 14/7 mm (OD/ID)	-	-	-	9021 */0	10,083 */50	10,088 */300	8228/1060	9727/1060	4802/1960	-	-	-	-	-
1b 14/7 mm (OD/ID)	-	-	-	7405/0	8928/50	7402/300	4687/1060	4521/1060	3162/1960	3178/2210	3263/2210	2391/2750	-	-
2a (Finger-like) 14/7 mm (OD/ID)	-	-	-	8151/0	10,767/50	9403/300	8344/1060	6963/1060	4915/1960	-	-	-	-	-
2b 14/7 mm (OD/ID)	-	-	-	7197 */0	7738 */50	7566 */300	7219 */1060	7654 */1060	5305/1960	4593/2210	4863/2210	3107/2750	-	-
3 10/4 mm (OD/ID)	-	-	-	9301 */0	9547 */50	7061/300	2114/1060	2290/1060	1029/1960	887/2210	933/2210	755/2750	-	-
4a 10/7 mm (OD/ID)	4125 */0	4745 */150	-	5826 */150	6788 */200	-	-	-	-	-	7319 */200	5066/480	4349/480	480/715
4b (Finger-like) 10/7 mm (OD/ID)	3047/0	2498/150	2967 **/850	4921 **/850	2793 **/900	248 **/1150	-	-	-	-	-	-	-	-
5 (Finger-like) 10/7 mm (OD/ID)	2746/0	2253/150	1762/850	3586/850	3047/900	2950/1150	-	-	-	-	-	-	-	-

* Nitrogen is out of measurement range, a minimum nitrogen flow of 0.200 ml/min is considered. ** Membrane is in a Fluidized-bed.

References

1. Yang, L.; Ge, X.; Wan, C.; Yu, F.; Li, Y. Progress and perspectives in converting biogas to transportation fuels. *Renew. Sustain. Energy Rev.* **2014**, *40*, 1133–1152. [CrossRef]

2. Gallucci, F.; Fernandez, E.; Corengia, P.; van Sint, M.; Annaland, M.V.; van Sint, M. Recent advances on membranes and membrane reactors for hydrogen production. *Chem. Eng. Sci.* **2013**, *92*, 40–66. [CrossRef]

3. Plazaola, A.A.; Tanaka, D.A.P.; Annaland, M.v.; Gallucci, F. Recent Advances in Pd-Based Membranes for Membrane Reactors. *Molecules* **2017**, *22*, 51. [CrossRef] [PubMed]

4. Uemiya, S.; Sato, N.; Ando, H.; Matsuda, T. Steam reforming of methane in a hydrogen-permeable membrane reactor. *Appl. Catal.* **1991**, *67*, 223–230. [CrossRef]

5. Seelam, P.K.; Liguori, S.; Iulianelli, A.; Pinacci, P.; Calabrò, V.; Huuhtanen, M.; Keiski, R.; Piemonte, V.; Tosti, S.; De Falco, M.; et al. Hydrogen production from bio-ethanol steam reforming reaction in a Pd/PSS membrane reactor. *Catal. Today* **2012**, *193*, 42–48. [CrossRef]

6. Islam, M.A.; Ilias, S. Steam Reforming of Methanol in a Pd-Composite Membrane Reactor Steam Reforming of Methanol in a Pd-Composite Membrane Reactor. *Sep. Sci. Technol.* **2012**, *47*, 2177–2185. [CrossRef]

7. Yun, S.; Lim, H.; Oyama, S.T. Experimental and kinetic studies of the ethanol steam reforming reaction equipped with ultrathin Pd and Pd-Cu membranes for improved conversion and hydrogen yield. *J. Memb. Sci.* **2012**. [CrossRef]

8. Okazaki, J.; Ikeda, T.; Pacheco, D.A.; Sato, K.; Suzuki, T.M.; Mizukami, F. An investigation of thermal stability of thin palladium-silver alloy membranes for high temperature hydrogen separation. *J. Memb. Sci.* **2011**, *366*, 212–219. [CrossRef]

9. Fernandez, E.; Helmi, A.; Coenen, K.; Melendez, J.; Viviente, J.L.; Tanaka, D.A.P.; Sint Annaland, M.; Gallucci, F. Development of thin Pd-Ag supported membranes for fluidized bed membrane reactors including WGS related gases. *Int. J. Hydrogen Energy* **2015**, *40*, 3506–3519. [CrossRef]

10. Mejdell, A.L.; Jøndahl, M.; Peters, T.A.; Bredesen, R.; Venvik, H.J. Experimental investigation of a microchannel membrane configuration with a 1.4 μm Pd/Ag23 wt.% membrane-Effects of flow and pressure. *J. Memb. Sci.* **2009**, *327*, 6–10. [CrossRef]

11. Liguori, S.; Iulianelli, A.; Dalena, F.; Piemonte, V.; Huang, Y.; Basile, A. Methanol steam reforming in an Al 2 O 3 supported thin Pd-layer membrane reactor over $Cu/ZnO/Al_2O_3$ catalyst. *Int. J. Hydrogen Energy* **2013**, *39*, 18702–18710. [CrossRef]

12. Abu, H.W.; Hawa, E.; Paglieri, S.N.; Morris, C.C.; Harale, A.; Way, J.D. Application of a Pd–Ru composite membrane to hydrogen production in a high temperature membrane reactor. *Sep. Purif. Technol.* **2015**, *147*, 388–397. [CrossRef]

13. Iulianelli, A.; Liguori, S.; Huang, Y.; Basile, A. Model biogas steam reforming in a thin Pd-supported membrane reactor to generate clean hydrogen for fuel cells. *J. Power Sources* **2015**, *273*, 25–32. [CrossRef]

14. Van Delft, Y.C.; Sumbharaju, R.; Meyer, D.F.; de Groot, A.; Sari, M. Steam reforming of methane in a bench-scale membrane reactor at realistic working conditions. *Catal. Today* **2012**, *193*, 74–80. [CrossRef]

15. Shirasaki, Y.; Tsuneki, T.; Ota, Y.; Yasuda, I.; Tachibana, S.; Nakajima, H.; Kobayashi, K. Development of membrane reformer system for highly efficient hydrogen production from natural gas. *Int. J. Hydrogen Energy* **2009**, *34*, 4482–4487. [CrossRef]

16. Roses, L.; Gallucci, F.; Manzolini, G.; Annaland, M.v.; van Sint, M. Experimental study of steam methane reforming in a Pd-based fluidized bed membrane reactor. *Chem. Eng. J.* **2013**, *222*, 307–320. [CrossRef]

17. Spallina, V.; Matturro, G.; Ruocco, C.; Meloni, E.; Palma, V.; Fernandez, E.; Melendez, J.; Tanaka, P.; Viviente Sole, J.L.; Sint Annaland, M.; et al. Direct route from ethanol to pure hydrogen through autothermal reforming in a membrane reactor: Experimental demonstration, reactor modelling and design. *Energy* **2018**, *143*, 666–681. [CrossRef]

18. Tanaka, D.A.P.; Tanco, M.A.L.; Niwa, S.I.; Wakui, Y.; Mizukami, F.; Namba, T.; Suzuki, T.M. Preparation of palladium and silver alloy membrane on a porous α-alumina tube via simultaneous electroless plating. *J. Memb. Sci.* **2005**. [CrossRef]

19. De Nooijer, N.; Gallucci, F.; Pellizzari, E.; Melendez, J.; Tanaka, D.A.P.; Manzolini, G.; Sint Annaland, M. On concentration polarisation in a fluidized bed membrane reactor for biogas steam reforming: Modelling and experimental validation. *Chem. Eng. J.* **2018**, *348*, 232–243. [CrossRef]

20. ASTM International. *ASTM F316-03—Standard Test Methods for Pore Size Characteristics of Membrane Filters by Bubble Point and Mean Flow Pore Test*; ASTM International: West Conshohocken, PA, USA, 2014. [CrossRef]

21. Günther, C.; Prehn, V.; Wölfel, T. New Membrane Applications in Liquid and Gas Seperation. In Proceedings of the 15th International Conference Inorganic Membranes, Dresden, Germany, 18–22 June 2018.

22. Peters, T.A.; Stange, M.; Bredesen, R. On the high pressure performance of thin supported Pd-23%Ag membranes-Evidence of ultrahigh hydrogen flux after air treatment. *J. Memb. Sci.* **2011**, *378*, 28–34. [CrossRef]

23. Mejdell, A.L.; Klette, H.; Ramachandran, A.; Borg, A.; Bredesen, R. Hydrogen permeation of thin, free-standing Pd/Ag23% membranes before and after heat treatment in air. *J. Memb. Sci.* **2008**, *307*, 96–104. [CrossRef]

24. Yang, L.; Zhang, Z.; Gao, X.; Guo, Y.; Wang, B. Changes in hydrogen permeability and surface state of Pd–Ag/ceramic composite membranes after thermal treatment. *J. Membr. Sci.* **2005**, *252*, 145–154. [CrossRef]

25. Roa, F.; Way, J.D. The effect of air exposure on palladium–copper composite membranes. *Appl. Surf. Sci.* **2005**, *240*, 85–104. [CrossRef]

26. Zemlyanov, D.; Klötzer, B.; Gabasch, H.; Smeltz, A. Kinetics of Palladium Oxidation in the mbar Pressure Range: Ambient Pressure XPS Study. *Topics Catal.* **2013**, *56*. [CrossRef]

27. Rollett, A.; Humphreys, F.; Rohrer, G.S.; Hatherly, M. *Recrystallization and Related Annealing Phenomena*, 2nd ed.; Pergamon Press: Oxford, UK, 2004. [CrossRef]

28. Abu, H.W.; Hawa, E.; Paglieri, S.N.; Morris, C.C.; Harale, A.; Way, J.D. Identi fi cation of thermally stable Pd-alloy composite membranes for high temperature applications. *J. Memb. Sci.* **2014**, *466*, 151–160. [CrossRef]

29. Melendez, J.; de Nooijer, N.; Coenen, K.; Fernandez, E.; Viviente, J.L.; Annaland, M.V.; Arias, P.L.; PachecoTanaka, D.A.; Gallucci, F. Effect of Au addition on hydrogen permeation and the resistance to H2S on Pd-Ag alloy membranes. *J. Memb. Sci.* **2017**, *542*, 329–341. [CrossRef]

30. Peters, T.A.; Carvalho, P.A.; van Wees, J.F.; Overbeek, J.P.; Sagvolden, E.; van Berkel, F.P.F.; Løvvik, O.M.; Bredesen, R. Leakage evolution and atomic-scale changes in Pd-based membranes induced by long-term hydrogen permeation. *J. Memb. Sci.* **2018**, *563*, 398–404. [CrossRef]

31. Kunii, D.; Levenspiel, O. Bubbling Fluidized Beds. In *Fluidization Engineering*; Elsevier: Amsterdam, The Netherlands, 1991. [CrossRef]

32. Stuhr, U.; Striffler, T.; Wipf, H.; Natter, H.; Wettmann, B.; Janssen, S.; Hempelmann, R.; Hahn, H. An investigation of hydrogen diffusion in nanocrystalline Pd by neutron spectroscopy. *J. Alloys Compd.* **1997**, *254*, 393–396. [CrossRef]

33. Bryden, K.J.; Ying, J.Y. Nanostructured palladium–iron membranes for hydrogen separation and membrane hydrogenation reactions. *J. Membr. Sci.* **2002**, *203*, 29–42. [CrossRef]

34. Guazzone, F.; Ma, Y.H. Leak Growth Mechanism in Composite Pd Membranes Prepared by the Electroless Deposition Method. *AIChE J.* **2008**, *54*, 487–494. [CrossRef]

35. Peters, T.A.; Tucho, W.M.; Ramachandran, A.; Stange, M.; Walmsley, J.C.; Holmestad, R.; Borg, A.; Bredesen, R. Thin Pd-23%Ag/stainless steel composite membranes: Long-term stability, life-time estimation and post-process characterisation. *J. Memb. Sci.* **2009**, *326*, 572–581. [CrossRef]

36. Haslam, A.J.; Phillpot, S.R.; Wolf, D.; Moldovan, D.; Gleiter, H. Mechanisms of grain growth in nanocrystalline fcc metals by molecular-dynamics simulation. *Mater. Sci. Eng. A* **2001**, *318*, 293–312. [CrossRef]

37. Helmi, A.; Fernandez, E.; Melendez, J.; Alfredo, D.; Tanaka, P.; Gallucci, F.; van Sint Annaland, M. Fluidized bed membrane reactors for ultra pure H$_2$ production—A step forward towards commercialization. *Molecules* **2016**, *21*, 376. [CrossRef] [PubMed]

38. Arratibel, A.; Tanaka, A.P.; Laso, I.; Annaland, M.v.; Gallucci, F.; Pacheco, A. Development of Pd-based double-skinned membranes for hydrogen production in fluidized bed membrane reactors. *J. Memb. Sci.* **2018**, *550*, 536–544. [CrossRef]